Heliyon 10 (2024) e25101

Contents lists available at ScienceDirect

Heliyon

journal homepage: www.cell.com/heliyon

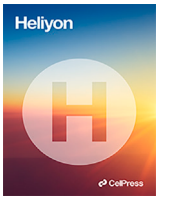

Research article

Magneto-convection of nanofluid flow over multiple rotating cylinders in a confined space with elastic walls and ventilated ports

Fatih Selimefendigil [a,b], Kaouther Ghachem [c], Hind Albalawi [d], Badr M. AlShammari [e], Taher Labidi [f], Lioua Kolsi [g,*]

[a] Department of Mechanical Engineering, College of Engineering, King Faisal University, Al Ahsa 31982, Saudi Arabia
[b] Department of Mechanical Engineering, Celal Bayar University, 45140 Manisa, Turkey
[c] Department of Industrial Engineering and Systems, College of Engineering, Princess Nourah bint Abdulrahman University, P.O. Box 84428, Riyadh 11671, Saudi Arabia
[d] Department of Physics, College of Sciences, Princess Nourah bint Abdulrahman University (PNU), P.O. Box 84428, Riyadh, 11671, Saudi Arabia
[e] Department of Electrical Engineering, College of Engineering, University of Ha'il, Ha'il City, Saudi Arabia
[f] Department of Software Engineering, College of Computer Engineering and Sciences, Prince Sattam bin Abdulaziz University, P.O. Box 151, Al-Kharj, 11942, Saudi Arabia
[g] Department of Mechanical Engineering, College of Engineering, University of Ha'il, Ha'il City 81451, Saudi Arabia

ARTICLE INFO

Keywords:
Elastic wall
Multiple rotating cylinders
Finite element method
Magnetic field
Optimization

ABSTRACT

In this study, convective heat transfer for nanofluid flow over multiple rotating cylinder in a confined space is analyzed under magnetic field while enclosure has one inlet and one outlet port. Three identical circular cylinder are used and the two walls of the cavity are considered to be elastic. The coupled fluid-structure interaction and magneto-convection problem is solved by finite element method. Impacts of rotational Reynolds number (Rew between -100 and 100), Hartmann number (Ha between 0 and 50), cylinder size (R between 0.001H and 0.11H) and Cauchy number (Ca between 10^{-8} and 10^{-3}) on the flow and thermal performance features are explored. The flow field and recirculation inside the cavity are significantly affected by the activation of rotation and magnetic field. The vortices are suppressed by increasing the strength of magnetic field and thermal performance is improved. Thermal performance of 56.6% is achieved by activation of magnetic field at the highest strength with rotations of the circular cylinders. When rotations are active, heat transfer rate is reduced while up to 40% reduction is obtained without magnetic field. Cylinder size has the highest impact on the overall thermal performance improvement while up to 132% enhancements are achieved. The contribution of elastic walls on the thermal performance is slight while less than 5% improvements in the average heat transfer is obtained. An optimization study leads to 12.7% higher thermal performance improvements as compared to best case of parametric computational fluid dynamics simulation results while the optimum values of (Rew, Ha, R) is obtained as (-80.66, 50, 0.11H).

* Corresponding author.
E-mail addresses: fgil@kfu.edu.sa (F. Selimefendigil), kgmaatki@pnu.edu.sa (K. Ghachem), hmalbalawi@pnu.edu.sa (H. Albalawi), bms.alshammari@uoh.edu.sa (B.M. AlShammari), t.labidi@psau.edu.sa (T. Labidi), l.kolsi@uoh.edu.sa (L. Kolsi).

https://doi.org/10.1016/j.heliyon.2024.e25101
Received 26 March 2023; Received in revised form 10 January 2024; Accepted 20 January 2024

Available online 26 January 2024

Nomenclature

B_0	magnetic field strength	ρ	density ... kg/m^3
Ca	Cauchy number	σ	electrical conductivity ... S/m
E	elastic modulus ... Pa	ω	rotational speed ... rad/s
Ha	Hartmann number		
h	heat transfer coefficient ... W/m^{2}K	*Subscripts*	
k	thermal conductivity ... W/mK	c	cold
n	unit normal vector	h	hot
Nu	Nusselt number	m	average
p	pressure ... Pa	nf	nanofluid
Pr	Prandtl number	p	solid particle
Re	Reynolds number		
Rew	non-dimensional rotational speed	*Abbreviations*	
T	temperature ... K	CW	clockwise
u, v	velocity components ... m/s	CCW	counter clockwise
w	port size ... m	COBYLA	Constrained Optimization
x, y	Cartesian coordinates ... m	BY	Linear Approximation
		FEM	finite element method
Greek Characters		HT	heat transfer
α	thermal diffusivity ... m^2/s	MGF	magnetic field
ϕ	solid volume fraction	NF	nanofluid
γ	inclination angle	SUPG	streamline upwind Petrov-Galerkin
ν	kinematic viscosity ... m^2/s	VEC	vented cavity

1. Introduction

Convective heat transfer (HT) for flow over circular cylinders (CCs) in confined environment are encountered in many thermal systems including heat exchangers, electronic cooling, material processing, flow control and many others. The CCs can be stationary, oscillating or rotating and their numbers can be varied in different applications [1]. In the literature, many studies considered the analysis of convective HT characteristics considering single CCs. Costa and Raimundo [2] used rotating CC in a square chamber under mixed convection while cylinder size, rotational speed and thermal conductivity on the HT enhancement were explored. They noted that the thermal performance of the enclosure were affected by the presence of the rotating CC and thermophysical properties of CC were important on the overall HT process. In many studies, the CC size and rotational speeds are considered as some of the important factors along with the location. There exist studies that consider the convection for flow over multiple CCs in confined spaces. Garmroodi et al. [3] used multiple CCs in a lid-driven enclosure as mixed convection problem under magnetic field (MGF). They considered different arrangement of the CCs while the vertical one provided the highest HT rates. Khanafer et al. [4] considered mixed convection in a cavity which is heated from left vertical wall and utilization of two rotating CCs. The combined effects of Reynolds number, Richardson number and cylinder rotation were explored. It was noted that direction of the rotations has significant impact on the overall thermal performance and flow pattern distributions within the chamber. Tahmasbi et al. [5], used two rotating CCs in a square cavity in mixed convection while porous media was considered as one of the HT enhancement techniques. Impacts of different rotations and directions were studied. It was noted that the highest HT contribution was achieved by using the optimized porous media. There are a few works that considered the installation of more than two rotating CCs in confined spaces [6,7].

Nano-enhanced MGF effects can be considered in thermal systems for effective flow control and thermal management. The MGF technology is used in diverse applications such as in biomedical, micro-fluidic pumps, energy harvesting, cooling and many others [8–12]. Nano-sized particles are used in base fluid for MGF applications. The nanofluid (NF) technology has been successfully implemented in diverse fields such as in energy storage, energy conversion, energy production, flow control, HT enhancement and many others [13–17]. In recent years, many advancements in applications and production of the NFs have been achieved along with the sophisticated modeling approach to better capture the NF impact on the thermal performance improvements [18–21]. When used with MGF, the effectiveness will be further improved due to the variation of thermophysical properties. In convective HT, magnetic NFs have been used for various cases of using external MGF such as uniform, partially active, spatially varying and time periodic [22–26]. Depending upon the application, MGF enhances the thermal transport and modulates the vortex size distribution within the system. In cavities with ventilation ports, MGF may affect those zones and increase the convective HT. The flow in ventilated cavities (VEC) has potential applications in drying, removing contaminants, electronic cooling and many other systems. In the VECs, flow field is very complex with occurrence of multiple vortices. The distribution and size of them can be adjusted by using external MGF and varying the strength and inclination of it as it has been shown in many studies [27–29].

The elastic deformation in thermo-fluid systems due to the pressure force exerted on the structure in fluid systems can alter the dynamics of convection as shown in previous studies [30–32]. The presence of elastic walls or objects in cavities results in local deformation of the cavity wall which will effect the flow pattern variations in the vicinity of those regions. Ghalambaz et al. [33]

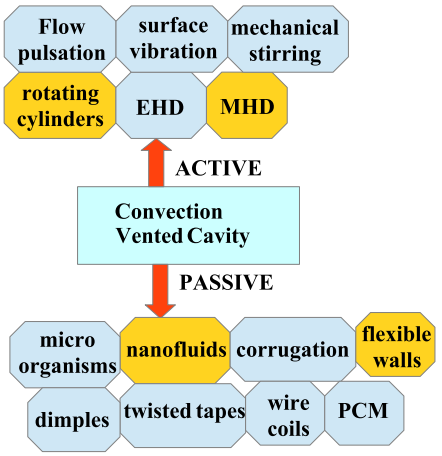

Fig. 1. Schematic view of the different HT enhancement techniques.

used an oscillating elastic fin in a square cavity where the fin was attached to hot vertical wall. It was noted that the oscillating amplitude can significantly contribute to the HT enhancement while a fin length of 0.2 was found as the best case for highest HT rate. In another study, Selimefendigil and Öztop [34] used an inner cylinder with elastic extension for the mixed convection in a 3D VEC system. By installing the cylinder and varying the elasticity of the extended part, the flow field and thermal patterns were found to be influenced. Ismael and Jasim [35] considered the mixed convection in a VEC with an elastic fin attached to the bottom wall. HT enhancement was obtained by using elastic fin as compared to rigid one while the average HT values were found to rise with higher Cauchy numbers.

In this study, we consider convective flow in a confined space in the presence of using three identical rotating CCs under MGF while the enclosure has ventilation ports. The elasticity of the bottom wall and right vertical wall is also considered. In Fig. 1, a schematic view of HT enhancement methods is given. Some of the available methods are used together for thermal performance improvement if the flow and convection control are the main objectives. In some applications, the flow over multiple rotating CCs are considered where the application is relevant in rotary type heat exchangers for waste heat recovery. The MGF can also be available within the system and its impacts on flow and HT should be considered. In both cases, the utilization of NF provides effective thermal performance improvements. In the literature, studies exist that consider the utilization of MGF in VEC and consideration of using CCs in VEC. As mentioned before, elastic walls and objects have also been considered in channels/cavities. However, there are a few studies that used more than two cylinders in channel /cavities.

This study combines the methods of using MGF, NF and multiple rotating cylinders in a VEC for flow control and thermal performance improvements. The elasticity of the enclosure walls is also taken into account. The MGF effects and multiple rotating cylinders may be present in the system or they can be used as tools for HT control. The coupled effects of rotations due to cylinders, wall elasticity of the confined space and MGF effects on flow and thermal behavior have never been studied for a VEC system. An optimization study is also conducted to provide the best operating parameters of the multiple rotating cylinder and magnetic field to achieve the highest HT rate of the VEC system. The outcomes can be considered for the initial design and development of new techniques for thermal management and performance improvements for convective flow over multiple rotating CCs in confined spaces where applications are found in electronic cooling, heat exchangers and many other HT equipments.

2. Modeling approach

2.1. Description of thermo-fluid system

Forced convection of NF in an elastic walled VEC system is considered by using three identical rotating CCs under MGF. The inlet port is installed on the upper left vertical wall with size of w while the exit port has the same size and located on the right part of the bottom wall as shown in Fig. 2. Cavity height is H while inlet/outlet port size is w = 0.25H. Cold fluid with uniform velocity is used at velocity of u_c and temperature of T_c. Left and top walls are assumed to be isothermal at $T = T_h$. The wall elasticity is considered for bottom and right walls. The elastic modulus, Poisson's ratio and density of solid material are E_s, ν_s and ρ_s. Three identical rotating CCs are used with their center locations at (xc1, yc1) = (0.25H, 0.35H), (xc2, yc2) = (0.25H+2R, 0.35H+4R) and (xc3, yc3) = (0.25H+4R,0.35H) while the cylinder radius is R which is varied between $0.001H$ and $0.11H$. The cylinders are adiabatic. The rotational speed of the CCs is ω while adiabatic walls are used for the CCs. The imposed MGF is uniform with magnitude of B_0 and having inclination of γ.

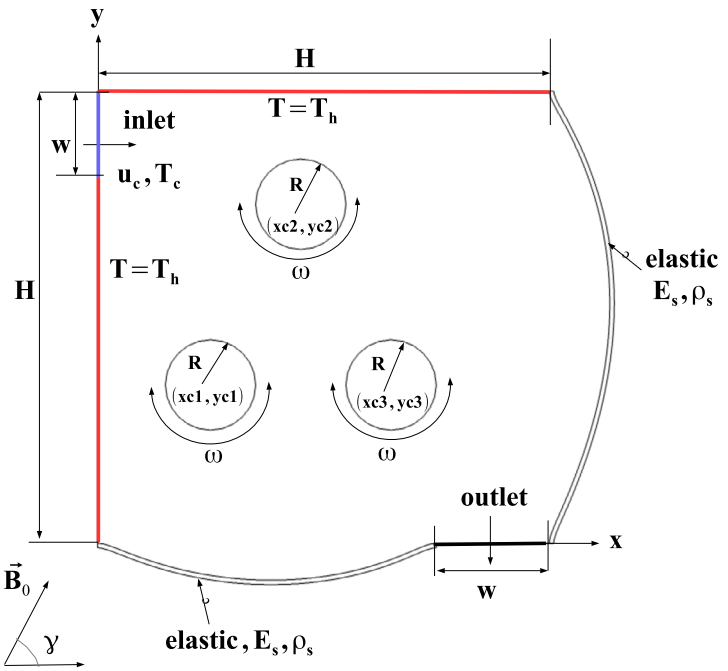

Fig. 2. Elastic walled VEC system with multiple rotating CCs under inclined MGF.

Table 1
Thermophysical properties of hybrid nanoparticles and base fluid [47].

Property name with unit	Ag	MgO	Water
ρ(kg/m^3)	10500	3560	997.1
C_p(J/kg K)	235	955	4179
k(W/m K)	429	45	0.62
μ(kg/m s)	-	-	8.55×10^{-4}

2.2. Governing equations and boundary conditions

In the current work, 2D and laminar flow is considered. Impacts of free convection, viscous dissipation and radiation effects are not taken into account. When MGF effects are used, induced MGF, displacement current effects and joule heating are not considered. As the HT fluid, NF of water having Ag-MgO hybrid nanoparticles is used with solid volume fraction of 0.02. Table 1 shows the thermophysical properties of nanoparticles and base fluid. A single phase mode of NF is adopted.

The conservation equations under the above given assumptions are stated as in equations (1)-(3):

$$\nabla.\mathbf{u} = 0 \tag{1}$$

$$(\mathbf{u}-\mathbf{w}).\nabla\mathbf{u} = -\frac{1}{\rho}\nabla P + \nu_f \nabla^2\mathbf{u} + \Gamma(\mathbf{u}\times\mathbf{B})\times\mathbf{B} + F \tag{2}$$

$$(\mathbf{u}-\mathbf{w})\nabla T = \alpha\nabla^2 T \tag{3}$$

where additional terms due to the MGF are seen in the momentum equations as $\frac{\Gamma B_0^2}{\rho}\left(v\sin(\gamma)\cos(\gamma) - u\sin^2(\gamma)\right)$ and $\frac{\Gamma B_0^2}{\rho}\left(u\sin(\gamma)\cos(\gamma) - v\cos^2(\gamma)\right)$, respectively. Here, Γ and γ are the electrical conductivity and inclination of MGF. In the FSI, equation for the solid zone is stated as in equation (4):

$$\rho_s \mathbf{a_s} = \nabla.\sigma_s + \mathbf{f_s}^b \tag{4}$$

where $\mathbf{f_s}^b$ denotes the body force while σ_s and $\mathbf{a_s}$ are the stress tensor and acceleration.

The relevant non-dimensional parameters are the Reynolds number (Re), Prandtl number, non-dimensional rotational speed (Rew), Hartmann number (Ha) and Cauchy number (Ca) which are stated as in the following equation (5):

$$\mathrm{Re} = \frac{u_c D_h}{\nu}, \quad \mathrm{Pr} = \frac{\nu}{\alpha}, \quad \mathrm{Ha} = B_0 H\sqrt{\frac{\Gamma}{\mu}}, \quad \mathrm{Rew} = \frac{\omega D_h^2}{\nu}, \quad \mathrm{Ca} = \frac{\rho u_c^2}{E^2} \tag{5}$$

Boundary conditions are stated as:

- At the inlet VEC, $u = u_c, v = 0, T = T_c$.
- At the exit of VEC, $\frac{\partial u}{\partial y} = 0, \quad v = 0, \quad \frac{\partial T}{\partial y} = 0$
- At the left and top wall of the VEC, $u = v = 0, \ T = T_h$
- For the left cylinder surface, $u = -\omega(y - yc1), v = \omega(x - xc1)$
- For the top cylinder surface, $u = -\omega(y - yc2), v = \omega(x - xc2)$
- For the right cylinder surface, $u = -\omega(y - yc3), v = \omega(x - xc3)$
- The cylinders are adiabatic, $\frac{\partial T}{\partial n} = 0$

For the FSI, the traction equilibrium ($\sigma_\mathbf{f} = \sigma_\mathbf{s}$) and displacement compatibility, ($\mathbf{d_f} = \mathbf{d_s}$) are used [36].

Local and average Nu are stated as in equation (6):

$$\mathrm{Nu}_s = \frac{h_s D_h}{k} = -\frac{D_h}{T_h - T_c}\frac{\partial T}{\partial n}_{wall}, \quad \mathrm{Nu}_m = \frac{1}{L_t}\int_0^H \mathrm{Nu}_s ds, \tag{6}$$

where s denotes the local coordinate and L_t denotes the total hot part of the VEC.

As the HT transfer fluid, hybrid NF is considered which uses water as base fluid with Ag-MgO hybrid nanoparticles. For this NF, correlations for thermal conductivity (k_{nf}) and viscosity (μ_{nf}) were developed based on experimental data and it is adopted here. They are given as in equation (7, 8) [37]:

$$k_{nf} = \left(\frac{0.1747\times10^5 + \phi}{0.1747\times10^5 - 0.1498\times10^6\phi + 0.1117\times10^7\phi^2 + 0.1997\times10^8\phi^3}\right)k_f, \tag{7}$$

$$\mu_{nf} = \left(1 + 32.795\phi - 7214\phi^2 + 714600\phi^3 - 0.1941\times10^8\phi^4\right)\mu_f, \tag{8}$$

where ϕ is the sum of the solid volume fraction of individual particles as in equation (9):

$$\phi = \phi_1 + \phi_2. \tag{9}$$

In this study, solid volume fraction of 0.02 is considered.

2.3. Solution method

The solution of the governing equation is made by using finite element method (FEM) with the arbitrary Lagrangian-Eulerian (ALE) technique [38,39]. The basic steps in modeling of fluid flow and heat transfer problems with FEM can be found in several references [40–42].

The approximation of field variables is made by using equation (10):

$$\begin{aligned} u &= \sum_{k=1}^{N^u}\Psi_k^{u,v}U_k, \ v = \sum_{k=1}^{N^v}\Psi_k^{u,v}V_k, \\ p &= \sum_{k=1}^{N^p}\Psi_k^{p}P_k, \ \ T = \sum_{k=1}^{N^u}\Psi_k^{T}T_k, \end{aligned} \tag{10}$$

where shape functions of $\Psi^{u,v}, \Psi^p$ and Ψ^T are used while U, V, P and T are the values at the nodes. Lagrange finite elements of various orders are considered. By using a weight function W, the weighted average of residual R is stated as in equation (11):

$$\int_V W R dv = 0. \tag{11}$$

To handle the problem of numerical instability, the SUPG is used. In the flow and HT module of the code, BiCGStab is used. To obtain convergence of the solver, a value of 10^{-7} is set.

2.4. Optimization method

The COBYLA (Constrained Optimization BY Linear Approximation) based optimization method is considered. The general problem by using PDE as an equality constraint is given in equation (12) [43,44]:

$$\begin{aligned} \underset{\psi}{\text{minimize}} \quad & \mathrm{f}(\Phi(\psi), \psi) \\ \text{subject to} \quad & \zeta(\Phi(\psi), \psi)) = 0, \\ & lb \le G(\Phi(\psi), \psi)) \le ub. \end{aligned} \tag{12}$$

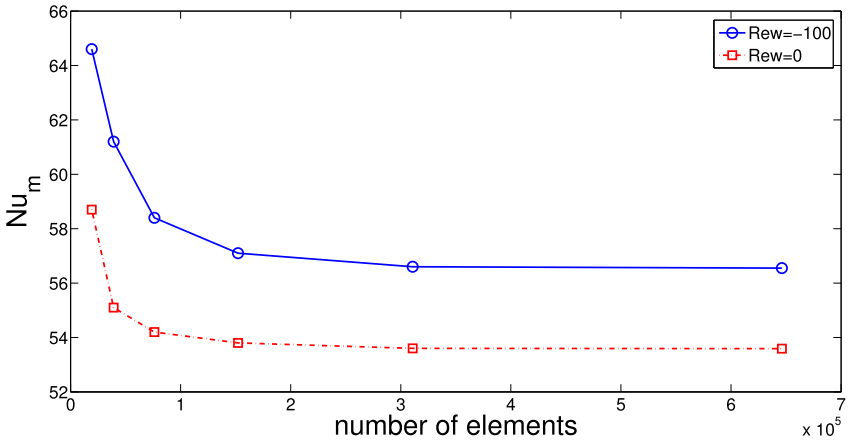

(a)

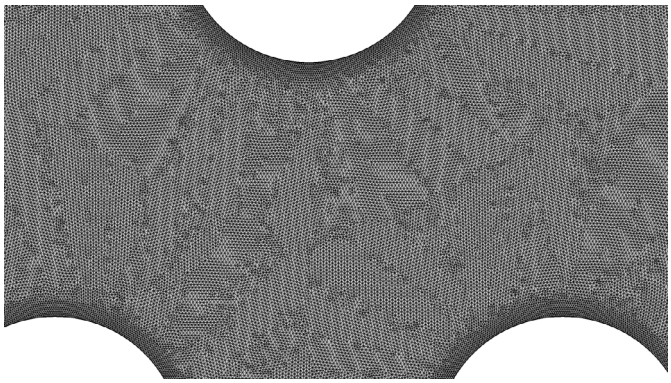

(b)

Fig. 3. Grid independence test results: Average Nu for different grid sizes at two rotational speed of the CCs.

In the above given representation, ψ and Φ are the control variables and PDE solutions while the constraints are denoted by G. The optimization method is a gradient-free and the interpolation at the vertices of a simplex is considered. At the iteration steps, it is performed within a trust zone. For the current problem, (Rew, Ha, R) parameter set is considered while the average HT from the hot surfaces is taken as the objective function.

2.5. Grid independence and code validation

Tests for grid independence are performed to obtain the optimal grid distribution. Fig. 3 (a) shows the average Nu versus element number considering two different rotations of the CCs. 320770 number of triangular type elements are used. Grid variation near the CCs is shown in Fig. 3 (b). The refinement of the grid near the cylinder walls is performed. Two different validation studies are performed. The first one is the convective HT study for cavity having elastic walls and thin flexible plate where reference study in Ref. [45] is used. Comparison of average Nu at two different Rayleigh numbers for flexible walled cavity is shown in Fig. 4 considering fixed values of $E^* = 8 \times 10^9$, $\rho s^* = 6000$ and baffle length of 0.8. The highest difference of 3.9% between the average Nu is obtained at $Ra = 10^4$. Another validation for convective HT in VEC is performed by using the reference study in Ref. [46] is considered. In the mentioned work, forced convection in a VEC having on inlet and one exit port is analyzed considering various values of Re. Comparison of average Nu at two different Re values are shown in Fig. 5. The variation between the results is below 3%. These results show that the current solver can handle convection problems in VEC and with elastic wall effects.

3. Results and discussion

Impacts of rotation of multiple inner cylinders and elasticity of the walls on the flow and convective HT characteristics are explored during forced convection of NF under MGF. Two walls are kept at isothermal while bottom and right walls are elastic-adiabatic. Three identical CCs are used which have rotational speed of ω. The numerical study is conducted for various values of Rew (between -100 and 100), Ha (between 0 and 50), cylinder sizes (R between 0.001H and 0.11H) and Ca (between 10^{-8} and 10^{-3}). An optimization study is also conducted for achieving the highest thermal performance. A uniform MGF is imposed with inclination

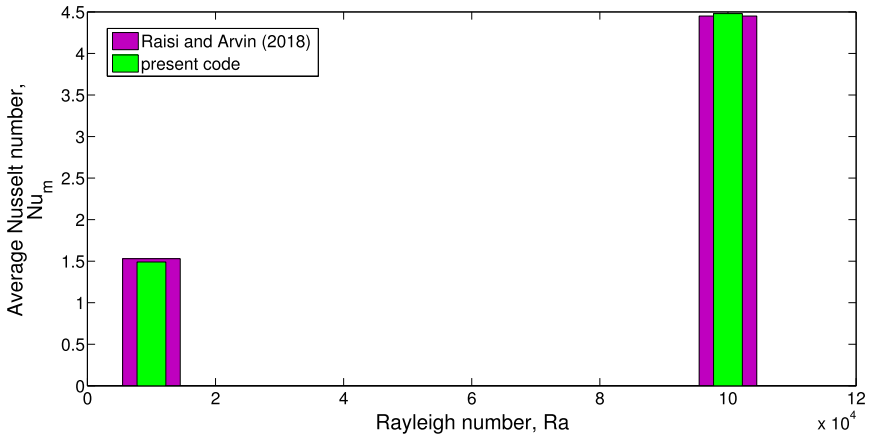

Fig. 4. Comparison of average Nu available in Ref. [45] for convective HT in an elastic walled cavity and a thin flexible plate at two different Rayleigh numbers ($E^* = 8 \times 10^9$, $\rho s^* = 6000$ and baffle length of 0.8).

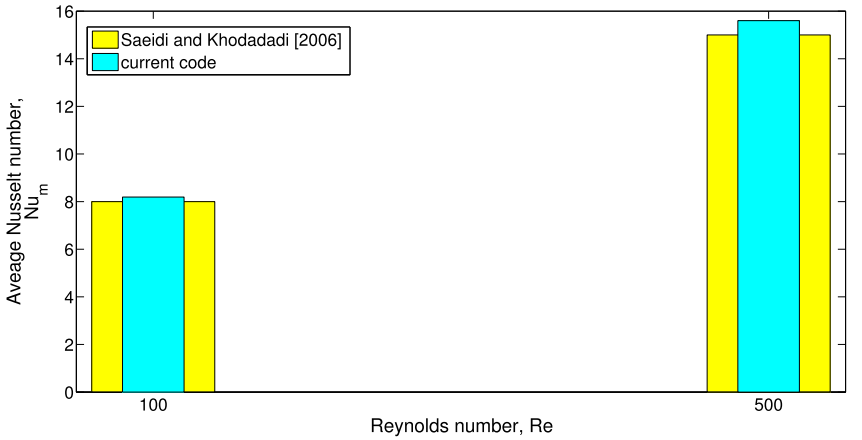

Fig. 5. Average Nu comparisons for convective HT in a VEC at two different Re. Results in Ref. [46] are used.

of 45 degrees with the horizontal while the Re is kept fixed at 1000. COBYLA based optimization technique is used to achieve the highest thermal performance.

3.1. Numerical simulation results

Streamline distributions are shown in Fig. 6 for varying rotational speeds of the multiple CCs at two different MGF strengths (Fig. 6 (a-e) for Ha = 0 and Fig. 6 (f-j) for Ha = 50). When there is no MGF, more flow recirculations are established within the cavity. The branching of fluid flow above and in between the cylinders are formed. For all rotational speeds, a corner vortex in the upper right part of the cavity is formed. Negative values of Rew indicates clockwise (CW) rotation of the CCs. For higher values of rotation in counter-CW (CCW), the flow branching in between the cylinders become more pronounced while vortex zones are formed behind the upper CC. On the upper and lower sides of the left CC, vortex zone size increases as well. For CW rotation of the CCs and rising its speed, the right corner vortex size becomes larger while at Rew = 100, a recirculation zone is formed near the bottom wall. When MGF is used at Ha = 50, due to the suppression of the vortices within the enclosure, only small variations are seen near the inlet zone where a small vortex is established. This is also reflected in the average Nu variations as shown in Fig. 7 (a, b) where the impacts of rotation in the existence of MGF effects at Ha = 50 will be slight. In the absence of MGF effects, the rotational velocity impact on the left heated wall is significant as compared to upper hot wall. When activating the rotations and increasing the speed, the average Nu generally reduces. The reduction amount becomes higher for CCW direction as compared to CW. The variations in the average Nu with Rew become 10.9% for CW rotation at the highest speed while it is 40% for CCW rotation of the cylinders without MGF effects. The variations in the average Nu with cylinder rotations become less than 5% under the MF effects at Ha = 50. This is attributed to the largely suppression of the vortex zone within the chamber having rotating CCs.

When MGF strength is gradually increased, the vortex size reduces for cases of rotating CCs (Fig. 8 (a-d)) or stationary CCs (Fig. 8 (e-h)). Due to the rotational effects of the left CC, two vortices are formed at Ha = 30 while the small vortex near the cylinder disappears at Ha = 50. For stationary CC case, the vortex below the upper CC remains but varies in extension up to Ha = 30 and is

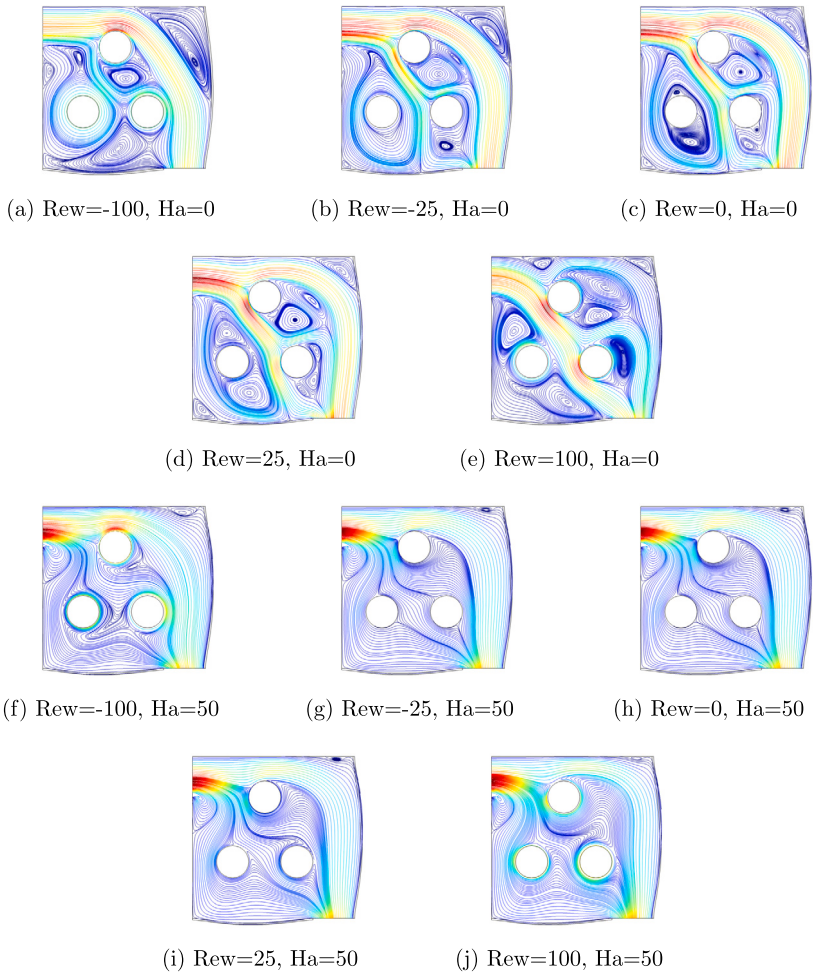

Fig. 6. Effects of Rew on the flow field variations at two different MGF strengths (a-e: Ha = 0), (f-j: Ha = 50) (Ca = 10^{-4}, R = 0.1H).

suppressed completely at Ha = 50. When rotations are active, the vortex zone in between the CCs are also reduced by using MGF and increasing its strength. Significant suppression of recirculation zones is observed at Ha = 50 while vortex size and number control inside the chamber can be done effectively by adjusting the MGF strength. Thermal performance improvements are seen for the left wall with higher MGF strength while this part has the highest contribution to the HT. For the top wall, thermal performance improvement with higher MGF strength is slight which is below 3%. The overall Nu increment with highest MGF strength becomes 56.6% for rotating case at Rew = -100 (Fig. 9 (a)) while it is 49% for non-rotating case (Fig. 9 (b)). By activating rotations more vortices are formed especially in between the cylinders and therefore MGF potential to suppress them and to enhance the thermal transport becomes higher.

Rotating CCs with larger sizes have more impacts on the flow re-circulation within the chamber as shown in Fig. 10 (a-f) especially when MGF is absent (Fig. 10 (a-c). At Ha = 0 and with the smallest size of rotating CCs, a large recirculation zone is formed around the object while the upper right corner vortex size extension is higher. The vortices are formed in between the cylinders while additional branching of the fluid flow toward the outlet in between the cylinders is seen with larger size. As the main-flow branching toward the upper part is formed, the upper right corner vortex becomes smaller. Fig. 11 (a, b) and Fig. 12 (a, b) show the size influence of CCs on the average Nu variations for various cases of activation of rotation and MGF effects (Fig. 11 (a, b) for Rew = -100 and Fig. 12 (a, b) for Rew = 0). In all cases, the positive contribution of the size on the thermal performance improvement is seen for the left and for the upper hot walls. The impact is higher when MGF is not active and significant changes are obtained when increasing the value of size from R = 0.075H to R = 0.11H. This is attributed to the size reduction of the vortex of the upper wall of the cavity and local velocity enhancement of the NF with reduced gap between the cylinder surfaces (upper and left) for higher cylinder size (Fig. 10 (c)). These effects are more pronounced when MGF effects are weak. In overall, when rotations are active (Rew = -100), the enhancements in the HT rates with larger cylinder sizes becomes 105% and 22% at Ha = 0 and Ha = 50 while they are 132% and 19.5% for non-rotating CC case. The application of MGF at Ha = 50 largely reduces the potential of using higher CC size in convection.

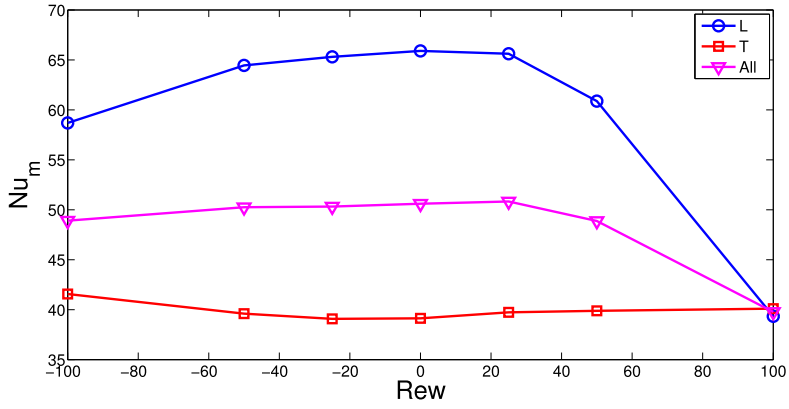

(a) Ha=0

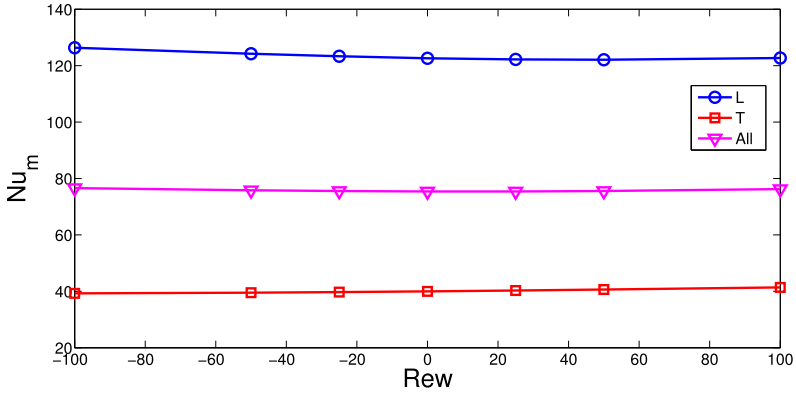

(b) Ha=50

Fig. 7. Impacts of CC rotational speed on the average Nu variations for left, top and all walls at Ha = 0 (a) and Ha = 50 (b) (Ca = 10^{-4}, R = 0.1H).

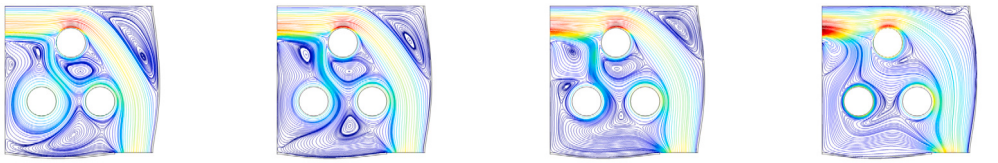

(a) Ha=0, Rew=-100 (b) Ha=20, Rew=-100 (c) Ha=30, Rew=-100 (d) Ha=50, Rew=-100

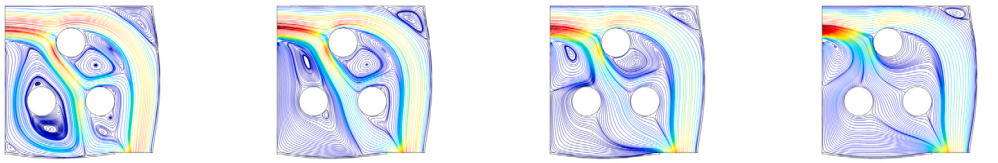

(e) Ha=0, Rew=0 (f) Ha=20, Rew=0 (g) Ha=30, Rew=0 (h) Ha=50, Rew=0

Fig. 8. Effects of MGF strength on the variation of streamlines with activation of rotations at Rew = -100 (a-d) and without rotations (e-h) (Ca = 10^{-4}, R = 0.1H).

Right and bottom part of the walls are made elastic. The deformation of the wall with exerted pressure due to the fluid motion is obtained and amount of deformation depends upon the fluid velocity and material of the wall. A higher Ca value denotes the case of using material with lower elastic modulus while Ca values are taken between 10^{-8} and 10^{-3}. Fig. 13 shows the streamline distributions for different values of Ca considering configurations with rotational (Fig. 13 (a-d)) and without rotational effects (Fig. 13 (e-h)). Higher values of Ca has impacts on the variation of vortices near the bottom wall and upper right corner. Due to the more deformation with higher Ca, the extension of vortex size (near the bottom part of the left CC) toward the bottom wall is seen while

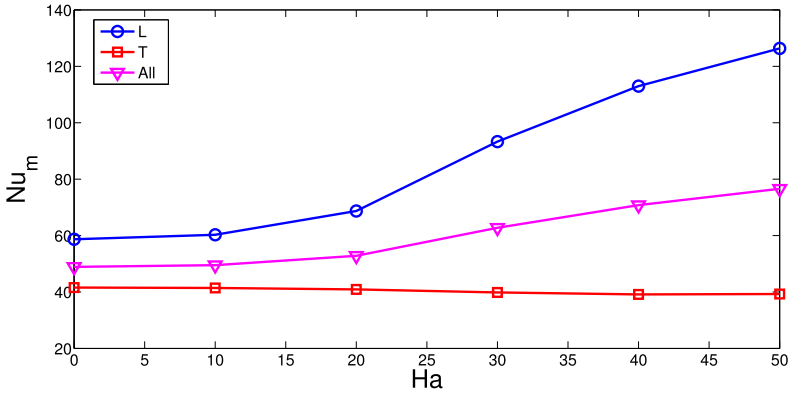

(a) Rew=-100

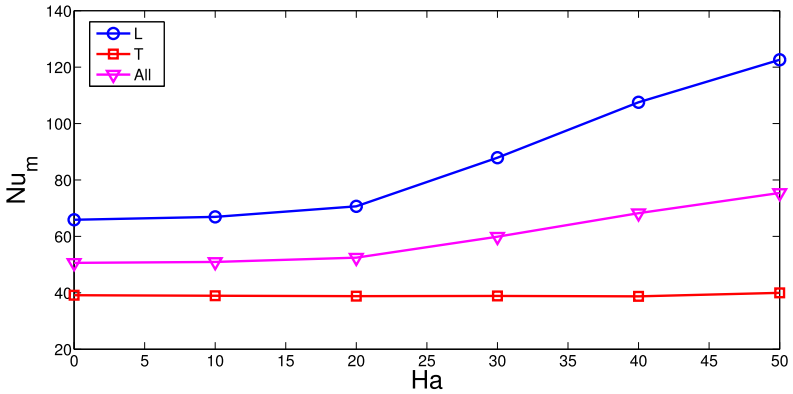

(b) Rew=0

Fig. 9. Average Nu versus Ha with rotations of the CCs at Rew = -100 (a) and without rotations (b) considering left, top and all hot walls (Ca = 10^{-4}, Rew = -100).

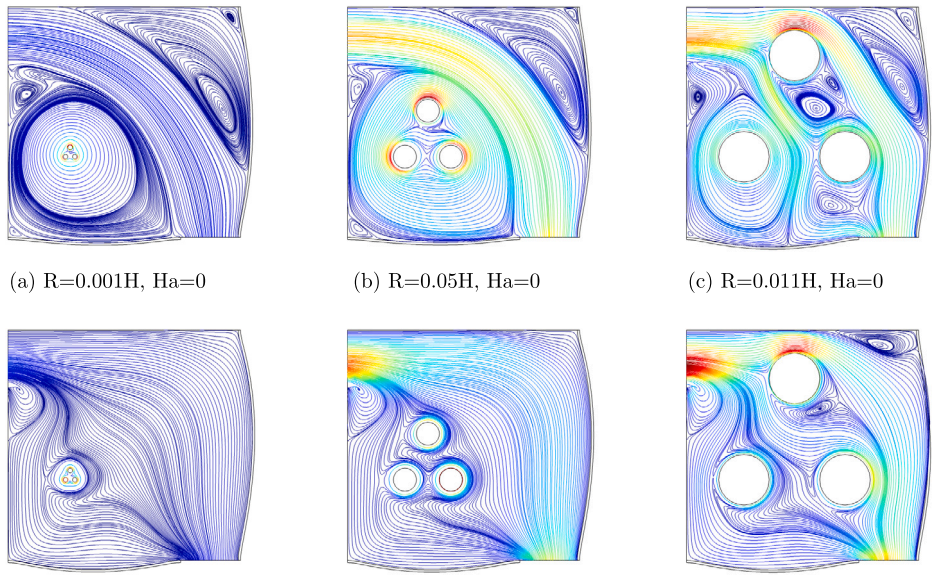

(a) R=0.001H, Ha=0 (b) R=0.05H, Ha=0 (c) R=0.011H, Ha=0

(d) R=0.001H, Ha=50 (e) R=0.05H, Ha=50 (f) R=0.011H, Ha=50

Fig. 10. Effects of rotating multiple CC size on the variation of streamlines without MGF (a-c) and under MGF (d-f) (Ca = 10^{-4}, Rew = -100).

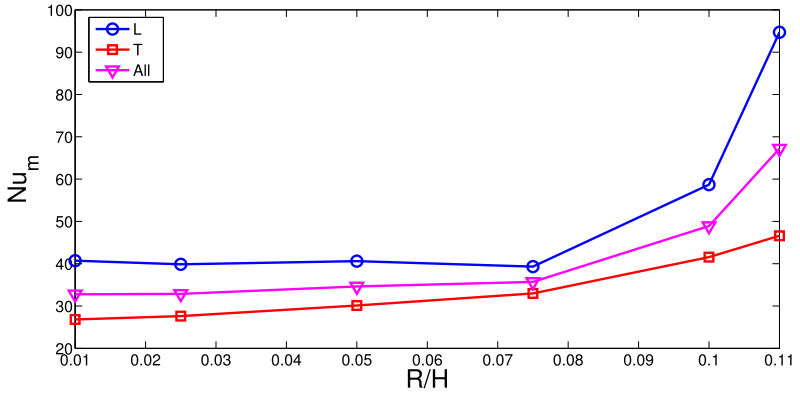

(a) Ha=0

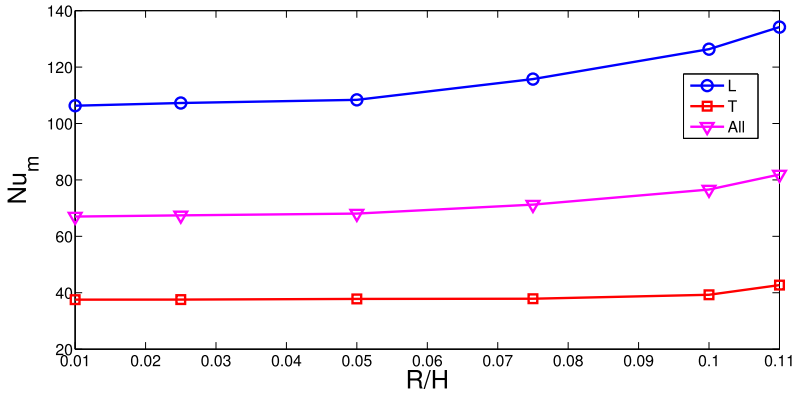

(b) Ha=50

Fig. 11. Average Nu versus size of the CCs for left, top and all hot walls considering no MGF (a) and with MGF at Ha = 50 (b) (Ca = 10^{-4}, Rew = -100).

the extension of the upper corner vortex is slightly increased due to the deformation of the right flexible wall. When rotations are activated, there is 5% and 2% variation of average Nu with varying the Ca values for the left wall and overall case (Fig. 14 (a)). When rotations are not used (Fig. 14 (b)), the average Nu changes with different Ca becomes below 2% for the bottom wall and overall case. As compared to MGF, cylinder size and rotational speed of the CCs, the elasticity of the wall is not that effective in HT control while variations in the average Nu becomes lower than 5%.

3.2. Optimization study results

An optimization study is conducted for achieving the highest HT performance of the system considering the constant Ca number case of 10^{-4}.

The lower and upper bounds are stated as in the following:

$$-100 \leq \mathrm{Rew} \leq 100, \quad 0 \leq \mathrm{Ha} \leq 50, \quad 0 \leq R \leq 0.11H. \tag{13}$$

The optimum values of (Rew, Ha, R) are obtained as (-80.66, 50, 0.11H). In parametric CFD, the most favorable condition in terms of thermal performance is expected to be at (Rew, Ha, R) = (-100, 50, 0.11H). In Fig. 15 (a-f), comparison results for the streamline and isotherm variations are seen between the parametric CFD and optimum case. The vortices are largely suppressed in between the cylinders and toward the upper right part of the cavity at Ha = 50 and at the optimum case. The extend of the right upper vortex is also reduced as the optimum as compared to case of Ha = 50 with parametric CFD. Isotherms show the intensification of the temperature gradients with highest MGF strength and optimum case near the hot walls. The average Nu is obtained as 80.2 in the parametric CFD which is almost 12.7% lower than the optimum one. When individual hot walls are compared, the value of Nu at the bottom wall is 13.6% higher and for the right wall is it 9.95% higher at the optimum case (Fig. 15 (g)).

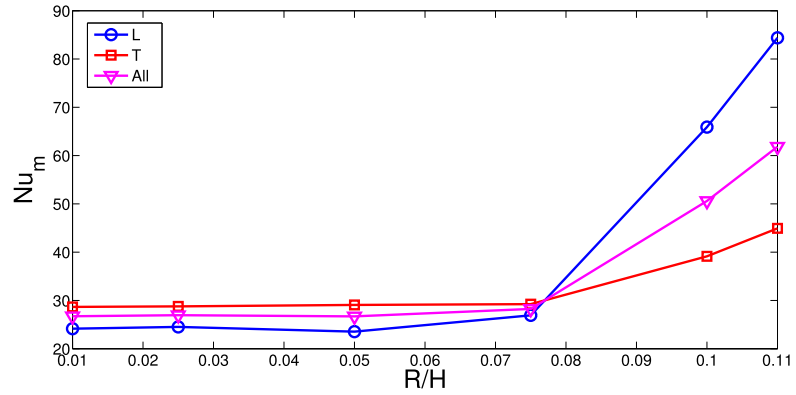

(a) Ha=0

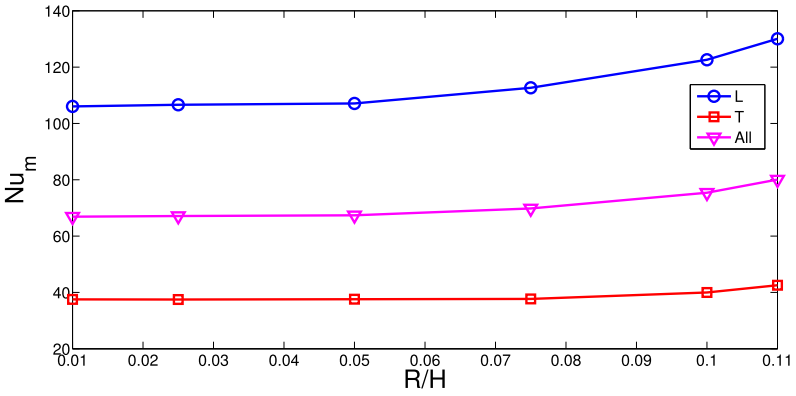

(b) Ha=50

Fig. 12. Average Nu versus size of the CCs for left, top and all hot walls considering no MGF (a) and with MGF at Ha = 50 (b) (Ca = 10^{-4}, Rew = 0).

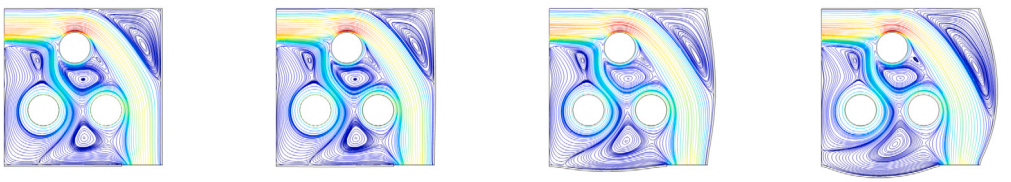

(a) Ca = 10^{-8}, Rew=-100 (b) Ca = 10^{-6}, Rew=-100 (c) Ca = 10^{-4}, Rew=-100 (d) Ca = 10^{-3}, Rew=-100

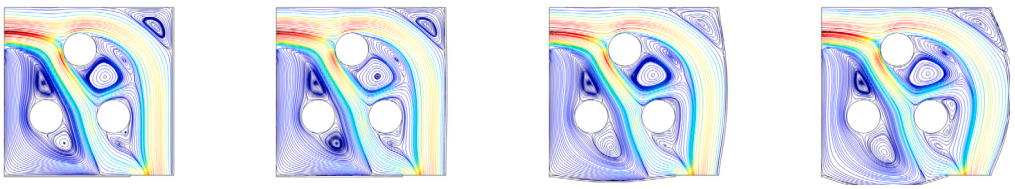

(e) Ca = 10^{-8}, Rew=0 (f) Ca = 10^{-6}, Rew=0 (g) Ca = 10^{-4}, Rew=0 (h) Ca = 10^{-3}, Rew=0

Fig. 13. Effects of Ca number on the streamline variations considering rotations of the CCs (a-d) and no-rotations (e-h) (Ha = 5, R = 0.1H).

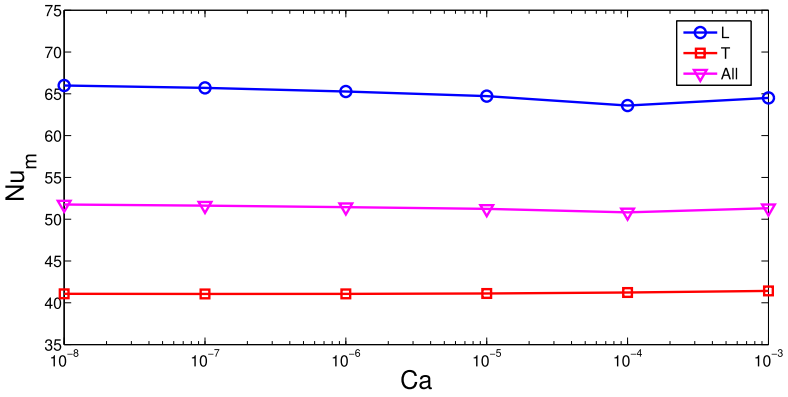

(a) Rew=-100

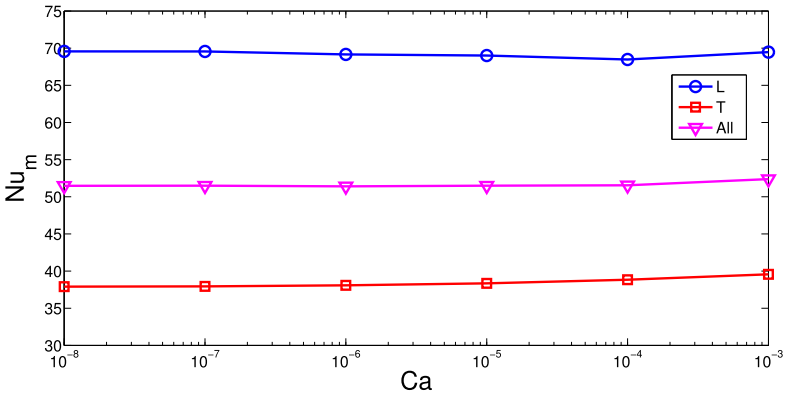

(b) Rew=0

Fig. 14. Impacts of Ca on the average Nu for left, top and all hot walls considering rotations at Rew = -100 (a) and no-rotations (b).

4. Conclusions

In this study, combined utilization of multiple rotating CCs and elastic walls are considered for convective HT in a VEC under MGF effects. The methods consider the use of several active and passive techniques together for flow control or it can be used in some practical applications such as waste heat recovery from rotating type heat exchanger. Following outcomes are achieved as:

- Branching of the fluid flow and formation of many vortices in between the CCs are formed by activation of rotation. This leads to reduction of thermal performance. Average Nu variations up to 10.9% and 40% are obtained for CW and CCW rotations at the highest speed without MGF effects.
- The impacts of cylinder rotation become less with MGF effects while less than 5% in the average Nu is obtained. However, increasing the MGF strength suppresses to multiple recirculations within the VEC and improves the thermal performance.
- Up to 56.6% HT improvement is obtained by using MGF strength at Ha = 50 for rotating case while it is 49% for non-rotating CC case.
- Larger rotating cylinder sizes improve the thermal performance and the impact is profound for the cases without MGF effects. Without MGF effects, up to 105% and 132% increments of average HT are obtained for rotating and non-rotating CC configurations by using the highest cylinder sizes.
- Even though elastic walls contribute to the local flow pattern variation near the deformed walls, the contributions to the overall thermal performance are not above 5% considering both rotating and non-rotating CC configurations.
- An optimization study is conducted and the optimum set of (Rew, Ha, R) parameters are obtained as (-80.66, 50, 0.11H). The optimum case leads to 12.7% higher HT values as compared to best case of parametric CFD.

The study can be extended to include different number of cylinders, different arrangement of them and thermally conductive cylinders. Effects of cylinder location on the thermal performance can also be investigated. MGF can also be imposed as non-uniform and partially active which can be considered as an extension of the present work.

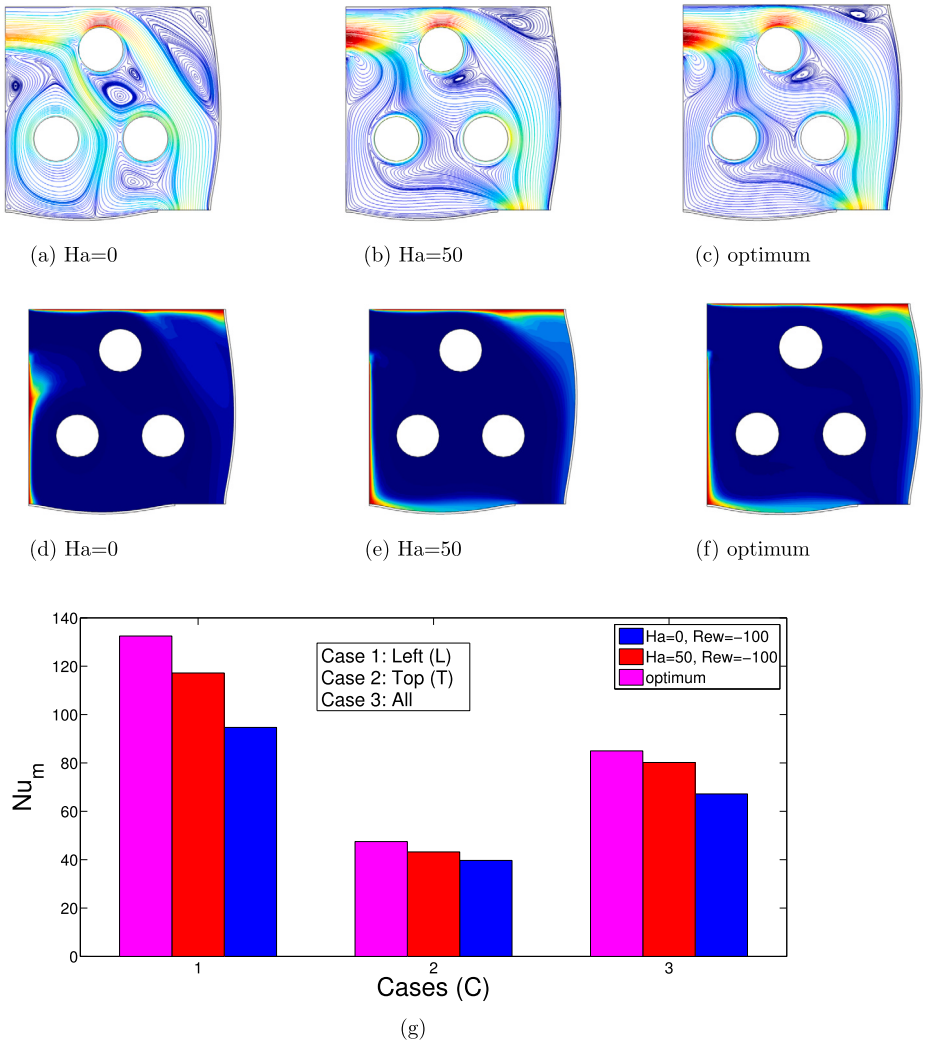

Fig. 15. Comparison of streamlines (a-c) and isotherms (d-f): parametric CFD at Ha = 0 and Ha = 50 (Rew = -100, R = 0.11H) and optimum case (c, f); Average Nu comparisons between the parametric CFD and optimum case (g).

CRediT authorship contribution statement

Fatih Selimefendigil: Writing – review & editing, Writing – original draft, Validation, Software, Methodology, Investigation, Formal analysis, Conceptualization. **Kaouther Ghachem:** Writing – review & editing, Writing – original draft, Methodology, Investigation, Funding acquisition, Formal analysis, Conceptualization. **Hind Albalawi:** Writing – review & editing, Writing – original draft, Investigation, Formal analysis. **Badr M. AlShammari:** Writing – review & editing, Writing – original draft, Investigation, Formal analysis. **Taher Labidi:** Writing – review & editing, Writing – original draft, Investigation, Formal analysis. **Lioua Kolsi:** Writing – review & editing, Writing – original draft, Methodology, Formal analysis, Conceptualization.

Declaration of competing interest

The authors declare that they have no known competing financial interests or personal relationships that could have appeared to influence the work reported in this paper.

Data availability

Not applicable.

Acknowledgement

This research project was funded by the Deanship of Scientific Research, Princess Nourah bint Abdulrahman University, through the Program of Research Project Funding After Publication, grant No (44- PRFA-P-17).

References

[1] S. Mehryan, E. Izadpanahi, M. Ghalambaz, A. Chamkha, Mixed convection flow caused by an oscillating cylinder in a square cavity filled with Cu–Al2O3/water hybrid nanofluid, J. Therm. Anal. Calorim. 137 (2019) 965–982.
[2] V. Costa, A. Raimundo, Steady mixed convection in a differentially heated square enclosure with an active rotating circular cylinder, Int. J. Heat Mass Transf. 53 (2010) 1208–1219.
[3] M.D. Garmroodi, A. Ahmadpour, F. Talati, Mhd mixed convection of nanofluids in the presence of multiple rotating cylinders in different configurations: a two-phase numerical study, Int. J. Mech. Sci. 150 (2019) 247–264.
[4] K. Khanafer, S. Aithal, K. Vafai, Mixed convection heat transfer in a differentially heated cavity with two rotating cylinders, Int. J. Therm. Sci. 135 (2019) 117–132.
[5] M. Tahmasbi, M. Siavashi, H.R. Abbasi, M. Akhlaghi, Mixed convection enhancement by using optimized porous media and nanofluid in a cavity with two rotating cylinders, J. Therm. Anal. Calorim. 141 (2020) 1829–1846.
[6] N. Shirani, D. Toghraie, M. Zarringhalam, M. Afrand, Numerical simulation of transient mixed convection of water–cu nanofluid in a square cavity with multiple rotating cylinders having harmonic motion, J. Therm. Anal. Calorim. 143 (2021) 4229–4248.
[7] F. Selimefendigil, H.F. Öztop, Magnetohydrodynamics forced convection of nanofluid in multi-layered U-shaped vented cavity with a porous region considering wall corrugation effects, Int. Commun. Heat Mass Transf. 113 (2020) 104551.
[8] O. Al-Habahbeh, M. Al-Saqqa, M. Safi, T.A. Khater, Review of magnetohydrodynamic pump applications, Alex. Eng. J. 55 (2016) 1347–1358.
[9] S. Yuan, Y. Huang, J. Zhou, Q. Xu, C. Song, G. Yuan, A high-efficiency helical core for magnetic field energy harvesting, IEEE Trans. Power Electron. 32 (2016) 5365–5376.
[10] M. Bahiraei, M. Hangi, Investigating the efficacy of magnetic nanofluid as a coolant in double-pipe heat exchanger in the presence of magnetic field, Energy Convers. Manag. 76 (2013) 1125–1133.
[11] A. Kitanovski, P.W. Egolf, Application of magnetic refrigeration and its assessment, J. Magn. Magn. Mater. 321 (2009) 777–781.
[12] B. Yu, Q. Gao, B. Zhang, X. Meng, Z. Chen, Review on research of room temperature magnetic refrigeration, Int. J. Refrig. 26 (2003) 622–636.
[13] A. Kasaeian, R. Daneshazarian, O. Mahian, L. Kolsi, A.J. Chamkha, S. Wongwises, I. Pop, Nanofluid flow and heat transfer in porous media: a review of the latest developments, Int. J. Heat Mass Transf. 107 (2017) 778–791.
[14] A.K. Hamzat, M.I. Omisanya, A.Z. Sahin, O.R. Oyetunji, N.A. Olaitan, Application of nanofluid in solar energy harvesting devices: a comprehensive review, Energy Convers. Manag. 266 (2022) 115790.
[15] B. Mehta, D. Subhedar, H. Panchal, Z. Said, Synthesis, stability, thermophysical properties and heat transfer applications of nanofluid–a review, J. Mol. Liq. (2022) 120034.
[16] A.H. Pordanjani, S. Aghakhani, M. Afrand, B. Mahmoudi, O. Mahian, S. Wongwises, An updated review on application of nanofluids in heat exchangers for saving energy, Energy Convers. Manag. 198 (2019) 111886.
[17] S. Mehryan, M. Ghalambaz, L.S. Gargari, A. Hajjar, M. Sheremet, Natural convection flow of a suspension containing nano-encapsulated phase change particles in an eccentric annulus, J. Energy Storage 28 (2020) 101236.
[18] A.H. Pordanjani, S. Aghakhani, M. Afrand, M. Sharifpur, J.P. Meyer, H. Xu, H.M. Ali, N. Karimi, G. Cheraghian, Nanofluids: physical phenomena, applications in thermal systems and the environment effects-a critical review, J. Clean. Prod. 320 (2021) 128573.
[19] M.U. Sajid, H.M. Ali, Recent advances in application of nanofluids in heat transfer devices: a critical review, Renew. Sustain. Energy Rev. 103 (2019) 556–592.
[20] A. Shahsavar, A.H. Alwaeli, N. Azimi, S. Rostami, K. Sopian, M. Arıcı, P. Estellé, S. Nižetić, A. Kasaeian, H.M. Ali, et al., Exergy studies in water-based and nanofluid-based photovoltaic/thermal collectors: status and prospects, Renew. Sustain. Energy Rev. 168 (2022) 112740.
[21] Z. Said, L.S. Sundar, A.K. Tiwari, H.M. Ali, M. Sheikholeslami, E. Bellos, H. Babar, Recent advances on the fundamental physical phenomena behind stability, dynamic motion, thermophysical properties, heat transport, applications, and challenges of nanofluids, Phys. Rep. 946 (2022) 1–94.
[22] A.A. Al-Rashed, L. Kolsi, H.F. Oztop, A. Aydi, E.H. Malekshah, N. Abu-Hamdeh, M.N. Borjini, 3d magneto-convective heat transfer in cnt-nanofluid filled cavity under partially active magnetic field, Physica E, Low-Dimens. Syst. Nanostruct. 99 (2018) 294–303.
[23] N. Biswas, M.K. Mondal, D.K. Mandal, N.K. Manna, R.S.R. Gorla, A.J. Chamkha, A narrative loom of hybrid nanofluid-filled wavy walled tilted porous enclosure imposing a partially active magnetic field, Int. J. Mech. Sci. 217 (2022) 107028.
[24] F. Selimefendigil, H.F. Öztop, F. Izadi, Non-uniform magnetic field effects on the phase transition dynamics for pcm-installed 3d conic cavity having ventilation ports under hybrid nanofluid convection, J. Build. Eng. 49 (2022) 104074.
[25] M.B. Gerdroodbary, M. Sheikholeslami, S.V. Mousavi, A. Anazadehsayed, R. Moradi, The influence of non-uniform magnetic field on heat transfer intensification of ferrofluid inside a t-junction, Chem. Eng. Process.-Process Intensif. 123 (2018) 58–66.
[26] S. Hussain, B.P. Geridonmez, Mixed bioconvection flow of ag-mgo/water in the presence of oxytactic bacteria and inclined periodic magnetic field, Int. Commun. Heat Mass Transf. 134 (2022) 106015.
[27] F. Selimefendigil, H.F. Öztop, Fluid-solid interaction of elastic-step type corrugation effects on the mixed convection of nanofluid in a vented cavity with magnetic field, Int. J. Mech. Sci. 152 (2019) 185–197.
[28] A. Kasaeipoor, B. Ghasemi, S. Aminossadati, Convection of cu-water nanofluid in a vented t-shaped cavity in the presence of magnetic field, Int. J. Therm. Sci. 94 (2015) 50–60.
[29] B.P. Geridönmez, H.F. Öztop, Effects of partial magnetic field in a vented square cavity with aiding and opposing of mwcnt–water nanofluid flows, Eng. Anal. Bound. Elem. 133 (2021) 84–94.
[30] F. Selimefendigil, H.F. Oztop, Mixed convection in a two-sided elastic walled and sio2 nanofluid filled cavity with internal heat generation: effects of inner rotating cylinder and nanoparticle's shape, J. Mol. Liq. 212 (2015) 509–516.
[31] S.A.M. Mehryan, M. Ghalambaz, M.A. Ismael, A.J. Chamkha, Analysis of fluid-solid interaction in MHD natural convection in a square cavity equally partitioned by a vertical flexible membrane, J. Magn. Magn. Mater. 424 (2017) 161–173.
[32] M.A. Ismael, H.F. Jasim, Role of the fluid-structure interaction in mixed convection in a vented cavity, Int. J. Mech. Sci. 135 (2018) 190–202.
[33] M. Ghalambaz, E. Jamesahar, M.A. Ismael, A.J. Chamkha, Fluid-structure interaction study of natural convection heat transfer over a flexible oscillating fin in a square cavity, Int. J. Therm. Sci. 111 (2017) 256–273.
[34] F. Selimefendigil, H.F. Öztop, Effects of an inner stationary cylinder having an elastic rod-like extension on the mixed convection of CNT-water nanofluid in a three dimensional vented cavity, Int. J. Heat Mass Transf. 137 (2019) 650–668.
[35] M.A. Ismael, H.F. Jasim, Role of the fluid-structure interaction in mixed convection in a vented cavity, Int. J. Mech. Sci. 135 (2018) 190–202.
[36] A. Al-Amiri, K. Khanafer, Fluid–structure interaction analysis of mixed convection heat transfer in a lid-driven cavity with a flexible bottom wall, Int. J. Heat Mass Transf. 54 (2011) 3826–3836.

[37] M.H. Esfe, A.A.A. Arani, M. Rezaie, W.-M. Yan, A. Karimipour, Experimental determination of thermal conductivity and dynamic viscosity of ag–mgo/water hybrid nanofluid, Int. Commun. Heat Mass Transf. 66 (2015) 189–195.
[38] J. Donea, S. Giuliani, J.-P. Halleux, An arbitrary lagrangian-eulerian finite element method for transient dynamic fluid-structure interactions, Comput. Methods Appl. Mech. Eng. 33 (1982) 689–723.
[39] D.T. Yaseen, S.M. Salih, M.A. Ismael, Effect of the lid-driven on mixed convection in an open flexible wall cavity with a partially heated bottom wall, Int. J. Therm. Sci. 188 (2023) 108213.
[40] R.W. Lewis, P. Nithiarasu, K.N. Seetharamu, Fundamentals of the Finite Element Method for Heat and Fluid Flow, John Wiley & Sons, 2004.
[41] J.N. Reddy, D.K. Gartling, The Finite Element Method in Heat Transfer and Fluid Dynamics, CRC Press, 2010.
[42] D. Pepper, The Intermediate Finite Element Method: Fluid Flow and Heat Transfer Applications, Routledge, 2017.
[43] M.J. Powell, A Direct Search Optimization Method that Models the Objective and Constraint Functions by Linear Interpolation, Springer, 1994.
[44] S.R. e Silva, R. Gomes, A. Falcao, Hydrodynamic optimization of the ugen: wave energy converter with u-shaped interior oscillating water column, Int. J. Marine Energy 15 (2016) 112–126.
[45] A. Raisi, I. Arvin, A numerical study of the effect of fluid-structure interaction on transient natural convection in an air-filled square cavity, Int. J. Therm. Sci. 128 (2018) 1–14.
[46] S.M. Saeidi, J. Khodadadi, Forced convection in a square cavity with inlet and outlet ports, Int. J. Heat Mass Transf. 49 (2006) 1896–1906.
[47] Y. Ma, R. Mohebbi, M. Rashidi, Z. Yang, MHD convective heat transfer of Ag-MgO/water hybrid nanofluid in a channel with active heaters and coolers, Int. J. Heat Mass Transf. 137 (2019) 714–726.